

BUILDINGS-TO-DISTRIBUTION NETWORK INTEGRATION TO ENABLE VOLTAGE REGULATION CONSIDERING RENEWABLE ENERGY RESOURCES

Hannah Fontenot¹, Krishna Sandeep Ayyagari², Bing Dong¹, Nikolaos Gatsis², Ahmad Taha²

¹Syracuse University, Syracuse, NY

²The University of Texas at San Antonio, San Antonio, TX

ABSTRACT

This paper develops a framework for buildings-to-distribution network (BtDN) integration. BtDN couples buildings, photovoltaic (PV) generation, and battery energy storage systems (BESS) to the power distribution network, using model predictive control to solve a joint optimization problem which minimizes building energy use while implementing reactive power control of PV and BESS inverters to maintain nodal voltage within prescribed limits at all times. The framework is tested in a pilot simulation study and improves upon a naïve control algorithm, showing 24% reduction in building energy usage, 40% reduction in network losses, and a complete elimination of voltage deviation.

INTRODUCTION

In the United States, buildings account for more than 70% of electricity use (DOE 2011). Within the building sector, heating, ventilation, and air conditioning (HVAC) accounts for approximately 50% of total building energy consumption. If the thermal energy storage capacity of buildings is properly managed, buildings can provide an enormous amount of demand response services to the distribution network in addition to reducing their energy usage and associated costs (Liu et al. 2018).

Due to the smart grid initiative, a large number of buildings equipped with photovoltaic devices (PVs) and battery energy storage systems (BESS) are connected to distribution networks. The increasing penetration of such distributed energy resources (DERs) and electric vehicles in distribution networks causes frequent and sizable voltage fluctuations. Maintaining voltages close to their nominal values as set by the ANSI C84.1 standard (ANSI 2016) is, therefore, a challenge in distribution networks. Thus more ancillary services are required in networks to maintain nodal voltages close to their nominal value (Smith et al. 2011). Also, due to the uncertain and intermittent nature of DERs, the traditional

slow-responding voltage devices like auto transformers, tap-changers, and shunt capacitors need to work harder to regulate voltages (Farivar et al. 2011). Hence the combined optimization of distribution networks and smart buildings has been emphasized by the U.S. Department of Energy in order to understand and take advantage of the multiple benefits and opportunities that such integration has to offer (DOE 2014).

There is a substantial body of work concerned with the optimization of distribution networks in conjunction with smart buildings. Many of these studies use a demand response scheme to implement building actions that also benefit the grid. For example, (Wei et al. 2016) develops a proactive building demand response scheme that integrates the actions of smart building HVAC systems with the scheduling of the distribution network so that buildings become a proactive participant in the demand response event rather than reacting to grid signals. This scheme achieved 10% reduction in generation costs and 20% reduction in building operation costs compared to a passive demand response scheme. Razmara et al. (2018) use a bidirectional optimization and control framework that exploits the flexibility of HVAC systems, PV generators, and BESS to provide demand response services to the grid in order to reduce load ramp-rates. The bidirectional control framework resulted in up to 26% reduction in monthly building electricity costs and 30% ramp-rate reduction, with probabilistic analyses showing similarly favorable results. In (Olama et al. 2018), buildings' load flexibility is exploited to provide frequency regulation services to the distribution network. Liu et al. (2019) develop a transactive distributed energy management system for community microgrids which schedules DERs and BESSs through iterative communication between the distribution network and individual buildings. This interaction enabled the controller to take actions that reduced voltage deviations by 2% and network losses by 9% even as building operating costs were reduced by up to 16% in a simulation study.

Recently there have been several studies that develop frameworks for full coupling of buildings and grid, in which buildings and the power grid are jointly optimized. (Taha et al. 2019) develops an integrated mathematical framework that explicitly couples commercial building dynamics to the dynamics of the power transmission network, using model predictive control (MPC) to simultaneously optimize building energy usage and grid frequency deviation. This building-to-grid framework achieved up to 43% total operational cost reduction, 17% HVAC consumption reduction, and up to 75% grid operational cost reduction in simulated case studies. (Liu et al. 2017) presents a mixed integer conic program that integrates building thermal dynamics into a network optimal power flow problem, optimizing operating costs, voltage deviation, network losses, and power factor at the point of common coupling. This framework achieved up to 16% operational cost reduction compared to autonomous control and up to 25% reduction in network losses. Jiang et al. (2018) develop an optimal scheduling method for smart building HVAC systems and on-load tap changer to optimize building energy costs and network losses and voltage deviations. In simulation studies, the proposed scheduling method resulted in up to 7% network loss reduction and 1% voltage deviation reduction under high building penetration and up to 5% network loss reduction under low building penetration, compared to conventional scheduling methods. Mirakhorli and Dong (2018) introduce a novel load aggregation method for a residential building-to-grid integrated system and use MPC to control residential loads in order to reduce the network's generation cost, peak load, and voltage drop. Case studies demonstrated a 21% reduction in generation cost, 17% reduction in peak load, and 22% reduction in building operational cost. The authors of (Badings et al. 2019) present a centralized MPC framework to model explicitly the hierarchical interactions between the transmission system operator, distribution system operator, and building energy storage units, as an extension of the work presented in (Taha et al. 2019). Using this framework, building-side storage flexibility was exploited to reduce grid frequency deviations by up to 50% overall and 64% for the distribution system operator alone.

Several of the works referenced above consider voltage regulation of distribution networks, either through control of DERs' active power or grid-level devices such as tap-changers and shunt capacitors. However, very few consider the flexibility of the PV and BESS inverters and the subsequent opportunity for reactive power support for voltage control. In particular, (Liu et al. 2017) and (Liu et al. 2019) considers reactive power support from BESS and distributed generators (other than PV) only.

Recent amendments of the IEEE 1547-2018 Standard (IEEE 2018) have allowed PV inverters to operate at non-unity power factor to provide reactive power support for voltage regulation in distribution networks; the benefits of PV inverter reactive power support are described in (Turitsyn et al. 2011). Therefore, it is important to understand the flexibility of PV inverters and BESS to provide reactive power support services for voltage regulation in a building-to-distribution network (BtDN) setup. Since these "smart" inverters can be operated at fast time-scales (less than 1 second), the lifetime of the conventional, slower-responding voltage regulation assets can be extended. Furthermore, enabling reactive power control of smart PV inverters can help to mitigate so-called "duck curve" issues caused by high penetration of renewable energy resources (Torabi et al. 2018).

In an effort to address the gaps in the relevant research, this paper proposes a framework to optimize building energy consumption, thermal set-point deviations, and network losses in a BtDN setup using MPC. Particularly, the objective of this paper is to investigate the benefits of reactive power support by PV and BESS inverters for nodal voltage regulation in a fully coupled BtDN integrated scheme. The framework proposed in this paper is fully flexible. Specifically, residential and commercial buildings as well as PV and BESS can be incorporated; in addition, the percentage of buildings which are equipped with DERs can be varied between zero and one hundred.

The rest of the paper is structured as follows. First, we present the mathematical models of building thermal dynamics, BESS and PV inverters, and the distribution network, and we describe their integration. Next, we formulate the joint optimization problem and detail the MPC algorithm that will be implemented in its solution. Then we present the results of a pilot simulation study and discuss their implications. We conclude the paper by discussing the study's limitations and outlining future research directions.

MATHEMATICAL MODELLING

In this section we develop mathematical models for buildings, PV inverters, battery energy storage systems, and the distribution network.

Building dynamics

A typical three-resistance and two-capacitance reduced-order thermal model, such as the one shown in Figure 1 (Taha et al. 2019), is considered for both the residential and commercial buildings in this integration framework. Typically, model parameters are tuned using an EnergyPlus building simulation model (DOE 2019); in this study, mean parameters were obtained from (Taha et

al. 2019) and (Lin et al. 2012) and validated using EnergyPlus. The mean parameters were then sampled to generate more buildings.

The dynamics of a building with temperature states T_{wall} and T_{zone} can be written in state space representation:

$$\dot{\mathbf{x}}_{b,l}(t) = \mathbf{A}_{b,l}\mathbf{x}_{b,l}(t) + \mathbf{B}_{u_{b,l}}\mathbf{u}_{b,l}(t) + \mathbf{B}_{w_{b,l}}\mathbf{w}_{b,l}(t) \quad (1)$$

where

- $\mathbf{x}_{b,l}(t) = [T_{\text{wall}}(t), T_{\text{zone}}(t)]^T$ is the state vector of building l at time t;
- $\mathbf{u}_{b,l}(t) = p_{\text{hvac},l}(t)$ is the control input (specifically, power delivered to the HVAC system) associated with building l at time t;
- $\mathbf{w}_{b,l}(t) = [T_{\text{amb}}(t), \dot{Q}_{\text{sol}}(t), \dot{Q}_{\text{int}}(t)]^T$ is the disturbance vector of building l at time t, which includes ambient temperature, building heat gains due to solar radiation, and internal heat gains due to occupants, lights, and equipment;
- $\mathbf{A}_{b,l}$, $\mathbf{B}_{u_{b,l}}$, and $\mathbf{B}_{w_{b,l}}$ are the system, input, and disturbance matrices associated with building l; these are time-invariant and depend on the physical characteristics of the individual building.

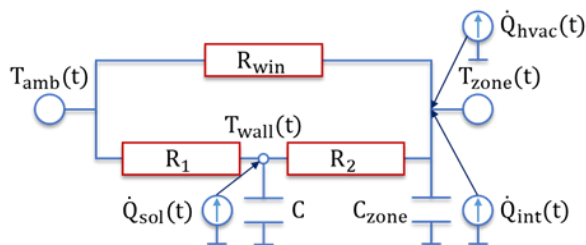


Figure 1 Reduced order building thermal model

The system represented in equation (1) can be converted to a discrete time system with appropriate sampling time T_{s_b} (60 sec); the discrete time dynamics are given by

$$\begin{aligned} \mathbf{x}_{b,l}(t+1) &= \tilde{\mathbf{A}}_{b,l}\mathbf{x}_{b,l}(t) + \tilde{\mathbf{B}}_{u_{b,l}}\mathbf{u}_{b,l}(t) \\ &\quad + \tilde{\mathbf{B}}_{w_{b,l}}\mathbf{w}_{b,l}(t) \end{aligned} \quad (2)$$

where

- $\tilde{\mathbf{A}}_{b,l} = (\mathbf{I}_2 - T_{s_b}\mathbf{A}_{b,l})^{-1}$, with \mathbf{I}_2 being the identity matrix of dimension 2;
- $\tilde{\mathbf{B}}_{u_{b,l}} = T_{s_b}\tilde{\mathbf{A}}_{b,l}\mathbf{B}_{u_{b,l}}$
- $\tilde{\mathbf{B}}_{w_{b,l}} = T_{s_b}\tilde{\mathbf{A}}_{b,l}\mathbf{B}_{w_{b,l}}$

The building states and inputs are constrained by upper and lower limits:

$$\mathbf{x}_{b,l}^{\min} \leq \mathbf{x}_{b,l}(t) \leq \mathbf{x}_{b,l}^{\max} \quad (3)$$

$$u_{b,l}^{\min} \leq u_{b,l}(t) \leq u_{b,l}^{\max} \quad (4)$$

Battery energy storage system

The battery energy storage system associated with building l is modeled linearly according to its state of charge (SOC) as follows:

$$x_{\text{bat},l}(t+1) = x_{\text{bat},l}(t) + k_g p_{\text{bat},l}(t) \quad (5)$$

where

- $x_{\text{bat},l}(t)$ is the SOC of battery l at time-step t;
- $p_{\text{bat},l}(t)$ is the active power drawn by the battery ($p_{\text{bat},l}(t) > 0$ denotes charging and $p_{\text{bat},l}(t) < 0$ denotes discharging);
- k_g is the duration of the time-step (it is convenient to choose k_g equal to T_{s_b}).

In addition to active power, the battery is capable of charging and discharging reactive power. The active and reactive power charged or discharged by the battery is constrained at each time-step t by the following:

$$p_{\text{bat},l}^2(t) + q_{\text{bat},l}^2(t) \leq (s_{\text{bat},l}^{\max})^2 \quad (6)$$

where

- $q_{\text{bat},l}(t)$ is the reactive power drawn by the battery, which follows the same charging/discharging convention as $p_{\text{bat},l}(t)$;
- $s_{\text{bat},l}^{\max}$ is the maximum apparent power rating of the battery inverter (this is a device operational specification).

The battery's operation is further constrained by limits on its charging/discharging power and SOC. Constraint (7) prolongs the life of the battery by preventing deep discharge and constraint (8) prevents overcharging.

$$x_{\text{bat},l}^{\min} \leq x_{\text{bat},l}(t) \leq x_{\text{bat},l}^{\max} \quad (7)$$

$$p_{\text{bat},l}^{\min} \leq p_{\text{bat},l}(t) \leq p_{\text{bat},l}^{\max} \quad (8)$$

PV inverter

Consider a PV inverter connected to building l with active power generation $p_{\text{pv},l}(t)$ which also has the capability to provide reactive power $q_{\text{pv},l}(t)$, respecting its maximum apparent power rating $s_{\text{pv},l}^{\max}$, by curtailing the active power generation by ratio $\alpha_{\text{pv},l}(t)$. The reactive power of this PV inverter is constrained in a similar manner to the BESS inverter:

$$\left((1 - \alpha_{\text{pv},l}(t)) p_{\text{pv},l}(t) \right)^2 + q_{\text{pv},l}^2(t) \leq (s_{\text{pv},l}^{\max})^2 \quad (9)$$

$$0 \leq \alpha_{\text{pv},l} \leq 1 \quad (10)$$

Due to the intermittency of solar irradiance, $p_{\text{pv},l}(t)$ is assumed to be an uncontrollable disturbance, whereas the reactive power $q_{\text{pv},l}(t)$ can be actively controlled. To facilitate reactive power control, the PV and battery

inverters are oversized to 105% of their rated apparent power.

Radial distribution network

A single-feeder radial distribution grid consisting of $N + 1$ buses and the lines connecting these buses is modeled by a tree graph as shown in Figure 2.

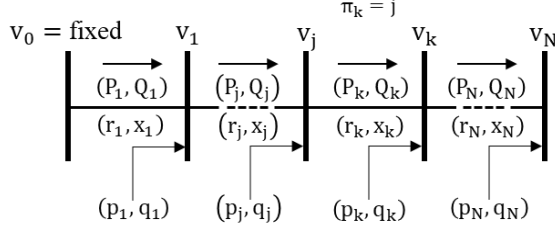


Figure 2 Radial network

The substation bus (root node) is indexed as node 0; this node connects to the external transmission network. Each node k has a parent node π_k and a set of child nodes, C_k . Node k is characterized by its squared magnitude voltage v_k , as well as the active and reactive power injections to the node ($p_k(t)$ and $q_k(t)$, respectively). Line k , which delivers power from node π_k to node k , is characterized by resistance r_k and reactance x_k , as well as active and reactive power flows $P_k(t)$ and $Q_k(t)$.

Using the simplified LinDistFlow approximation of the power flow equations, developed in (Baran and Wu 1989) and (Kekatos et al. 2015), along with some algebraic manipulations, the nodal voltages become a linear function of power injections:

$$\mathbf{v}(t) = \mathbf{R}\mathbf{p}(t) + \mathbf{X}\mathbf{q}(t) + \tilde{\mathbf{v}} \quad (11)$$

where

- $\mathbf{v}(t) = [v_1(t), \dots, v_N(t)]^T$ contains the squared magnitude voltage of each node at time t ;
- $\mathbf{p}(t) = [p_1(t), \dots, p_N(t)]^T$ contains the net active power injection to each node at time t ;
- $\mathbf{q}(t) = [q_1(t), \dots, q_N(t)]^T$ contains the net reactive power injection to each node at time t ;
- $\mathbf{R} := 2\mathbf{F}\text{diag}(\mathbf{r})\mathbf{F}^T$, $\mathbf{X} := 2\mathbf{F}\text{diag}(\mathbf{x})\mathbf{F}^T$ with $\mathbf{r}, \mathbf{x}, \mathbf{F}$ being determined by network parameters as defined in (Kekatos et al. 2015); and
- $\tilde{\mathbf{v}} = \mathbf{1}_N v_0$ where $\mathbf{1}_N$ is a vector of length N with each element being unity and v_0 is the squared magnitude voltage of the root node.

The per unit nodal voltages must satisfy the limits dictated by ANSI C84.1 (ANSI 2016) at each time t :

$$0.95^2 \leq v_k(t) \leq v_k^{\max} = 1.05^2 \quad \forall k, t \quad (12)$$

Building-to-distribution network integration

The buildings, PV generation devices, and battery energy storage systems are integrated to the distribution network through power balance equations (as illustrated in Figure 3).

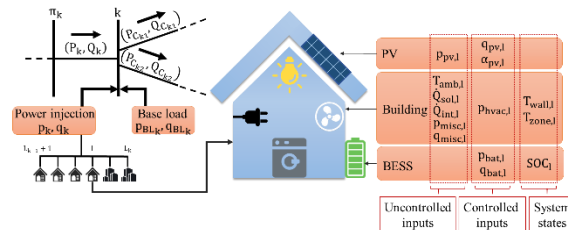


Figure 3 Buildings integrated into distribution network

Each node's active power injection $p_k(t)$ is a balance between the total power demand from all buildings served by the node (with node k serving $N_{b,k}$ buildings), the power generated by their PV devices, the active power charged or discharged by their battery devices, and the uncontrollable active power base load at that node. Similarly, the reactive power injection at node k , $q_k(t)$, is a balance between the total reactive power demand from all buildings, the reactive power charged or discharged by their PV and battery inverters, and the uncontrollable reactive power base load. These relationships are modeled mathematically in equations (13) and (14):

$$p_k(t) = \sum_{l=1}^{N_{b,k}} (p_{pv,l}(t) - p_{bat,l}(t) - p_{hvac,l}(t) - p_{misc,l}(t)) - p_{BL_k}(t) \quad (13)$$

$$q_k(t) = \sum_{l=1}^{N_{b,k}} (q_{pv,l}(t) - q_{bat,l}(t) - q_{misc,l}(t)) - q_{BL_k}(t) \quad (14)$$

where $p_{misc,l}(t)$ and $q_{misc,l}(t)$ denote the miscellaneous active and reactive power demand for building l . These miscellaneous loads can include lights, various devices, and plug loads. The HVAC reactive power q_{hvac} is not considered in equation (14) because it is assumed that each HVAC device incorporates a built-in capacitor to supply its own reactive power, as is standard in the industry.

PROBLEM FORMULATION

Model predictive control

Model predictive control (or receding horizon control) relies on the system dynamic model. At a time step t , the controller solves an optimization problem over a prediction horizon T_p , resulting in an optimal control profile $\mathbf{u}^* = \{\mathbf{u}(t), \dots, \mathbf{u}(t + T_p)\}$ consisting of T_p control actions. The first step of \mathbf{u}^* is implemented, after

which the horizon recedes by a time span T_h , the “current time” t becomes $t + T_h$, and the process repeats. MPC’s advantage lies in its ability to take into account future conditions when making control decisions for the present. The general form of an MPC optimization problem (\mathcal{P}_0) is as follows:

$$\begin{aligned} \min \quad & J = \sum_{\tau=t+1}^{t+T_h} f(\mathbf{x}(\tau), \mathbf{u}(\tau)) \\ \text{s.t.} \quad & \mathbf{x} \in X \\ & \mathbf{u} \in U \\ & \mathbf{x}(t+1) = \tilde{\mathbf{A}}\mathbf{x}(t) + \tilde{\mathbf{B}}_u\mathbf{u}(t) + \tilde{\mathbf{B}}_w\mathbf{w}(t) \quad (\mathcal{P}_0) \end{aligned}$$

In this study we apply a fully centralized approach to the joint optimization problem. The joint optimization problem (\mathcal{P}) is postulated as:

$$\begin{aligned} \min \quad & J = \frac{1}{T_p} \sum_{t=1}^{T_p} [\frac{1}{2v_0} \rho_{\text{loss}}(\mathbf{p}^T(t)\mathbf{R}\mathbf{p}(t) + \\ & \mathbf{q}^T(t)\mathbf{R}\mathbf{q}(t)) + \rho_{\epsilon_b} \epsilon_b(t)] \\ \text{over} \quad & \{\mathbf{p}_{\text{hvac}}(t), \mathbf{p}_{\text{bat}}(t), \mathbf{q}_{\text{bat}}(t), \mathbf{q}_{\text{pv}}(t), \boldsymbol{\alpha}_{\text{pv}}(t), \\ & \mathbf{x}_b(t), \mathbf{x}_{\text{bat}}(t), \mathbf{v}(t)\}_{t=1}^{T_p} \\ \text{s.t.} \quad & (2) - (14) \quad (\mathcal{P}) \end{aligned}$$

where

- $\mathbf{p}(t)$ and $\mathbf{q}(t)$ are vectors that collect the nodal active and reactive power injections $p_k(t), q_k(t)$ for each node k ;
- ρ_{loss} and ρ_{ϵ_b} are weights used to tune the relative importance of the grid and building objectives;
- $\mathbf{p}_{\text{hvac}}(t), \mathbf{p}_{\text{bat}}(t), \mathbf{q}_{\text{bat}}(t), \mathbf{q}_{\text{pv}}(t), \boldsymbol{\alpha}_{\text{pv}}(t), \mathbf{x}_b(t)$, and $\mathbf{x}_{\text{bat}}(t)$ are vectors collecting HVAC power consumption, battery active power charge/discharge, battery reactive power set-points, PV reactive power set-points, PV active power curtailment, building state, and battery state for each building l ;
- $\epsilon_b(t)$ is a vector that collects the temperature set-point violations for each building at time t ; and
- the other quantities are as previously defined.

In the objective function of (\mathcal{P}), the first term inside the summation penalizes the total network losses over the simulation duration. The second term penalizes temperature deviations within the buildings. Each objective is averaged over the entire simulation time. This joint loss function allows the controller to make decisions that simultaneously optimize the benefits to both the buildings and the distribution network.

Because we employ a centralized optimization method, the controller first aggregates all system data including model parameters for each building, BESS, PV, and the network; forecasted values for weather disturbances, miscellaneous building power demand, and nodal base loads (these are assumed to be known in advance); and limits on system states and input values. Then the joint problem (\mathcal{P}) is solved in an iterative fashion according to the MPC scheme, with final outputs including optimal control set-points for building HVAC systems, battery active power charging/discharging set-points, reactive power set-points for PV and battery inverters, and PV curtailment set-points for PV inverters.

SIMULATION

Benchmark algorithm

The centralized MPC algorithm is benchmarked against a naive rule-based control (RBC) algorithm. The algorithm consists of two heuristic sub-algorithms – one for the building and one for the battery. The building sub-algorithm controls the building HVAC power depending solely on the zone temperature: if the temperature is above the cooling set-point, HVAC power is increased; else HVAC power is set to zero. The battery sub-algorithm controls the battery charging/discharging power based on battery SOC and available PV power: if the available PV power is enough to satisfy building demand, then any remaining power is used to charge the battery (assuming the battery is not yet full – if it is full, any excess power is assumed curtailed). If building demand is greater than the PV power available, then the battery is discharged to help meet the demand (assuming the battery is not empty – if it is empty, then power is drawn from the grid to meet the building load). The RBC algorithm excludes reactive power control of the PV and battery.

Pilot simulation

A pilot simulation was performed to demonstrate the value of the BtDN framework. In this simulation, a 4-bus network serves 50 residential and 2 commercial buildings. The total simulation time is 24 hours, with the optimization being solved over a prediction horizon T_p of 6 hours; the horizon recedes $T_h = 1$ hour at each iteration. Building control horizon is 15 minutes; since the power generated by solar panels varies by 15% of its nameplate rating within one-minute intervals, we have assumed a control horizon of 1 minute for both PV and battery inverters (Wang et al. 2016).

With the LinDistFlow approximations for power distribution network, linear and quadratic constraints, and quadratic objective function, the problem (\mathcal{P}) is a quadratically constrained quadratic problem (QCQP) and can therefore be easily solved by off-the-shelf

solvers. The simulations for this study were performed using MATLAB/CVX (Grant and Boyd 2014) using the solver Gurobi (Gurobi 2019).

RESULTS AND DISCUSSION

The results of the pilot simulation are presented in Figures 4 and 5. In Figure 4, the top row shows the results for the RBC algorithm; the bottom row shows the MPC results. The left column plots the voltage at the terminal node over the course of the simulation (solid blue line) with the ANSI C84.1 limits represented by dashed black lines. The solid orange line represents the voltage in a scenario where reactive power support (Q-support) is disabled. The right column plots the power consumed by a single commercial building HVAC system (solid blue line) along with ambient temperature (dotted orange line), zone temperature (dot-dashed green line), and temperature set-points (dashed black lines). Here we note that there is a single line for HVAC power in the predictive control case because the power consumption curves for the two MPC scenarios (with and without Q-support) are extremely similar. The same applies for the building indoor temperature.

In this study, the network power flows and voltages are calculated using the LinDistFlow approximation of nonlinear power flow equations. The control set-points computed in the centralized optimization are validated using the actual nonlinear power flow (Z-bus method) outlined in (Bazrafshan and Gatsis 2018). In particular,

the nodal voltages and resulting average thermal losses are computed using the Z-bus method.

Under the RBC algorithm, nodal voltage drops gradually throughout the day until 6 pm, dipping below the lower limit once around 5:30 pm. This is due to the fact that the residential loads are gradually increasing in the evening, at the same time that PV generation naturally decreases. In addition, the voltage profile contains several sudden changes, such as spikes or sudden steep drops. These instabilities are caused by changes in outdoor temperature and solar radiation which, when combined with building temperature set-point changes, cause building loads to change drastically, placing strain on the distribution network.

Under MPC the voltage exhibits a much more stable profile; the voltage never drops below 0.98 per unit (when Q-support is enabled) or 0.96 per unit (when Q-support is disabled) and experiences fewer sudden changes. Furthermore, the changes that are present in the voltage profile are less drastic than those in the RBC profile, whether Q-support is present or not.

With Q-support enabled, the MPC algorithm utilizes reactive power control of PV and BESS inverters to support the grid throughout the day and maintain per unit voltage as close to unity as possible (this is seen in Figure 5). Even with Q-support disabled, the MPC algorithm is still able to improve the network voltage and prevent it from falling below the lower limit. MPC's predictive ability allows the controller to take actions to mitigate

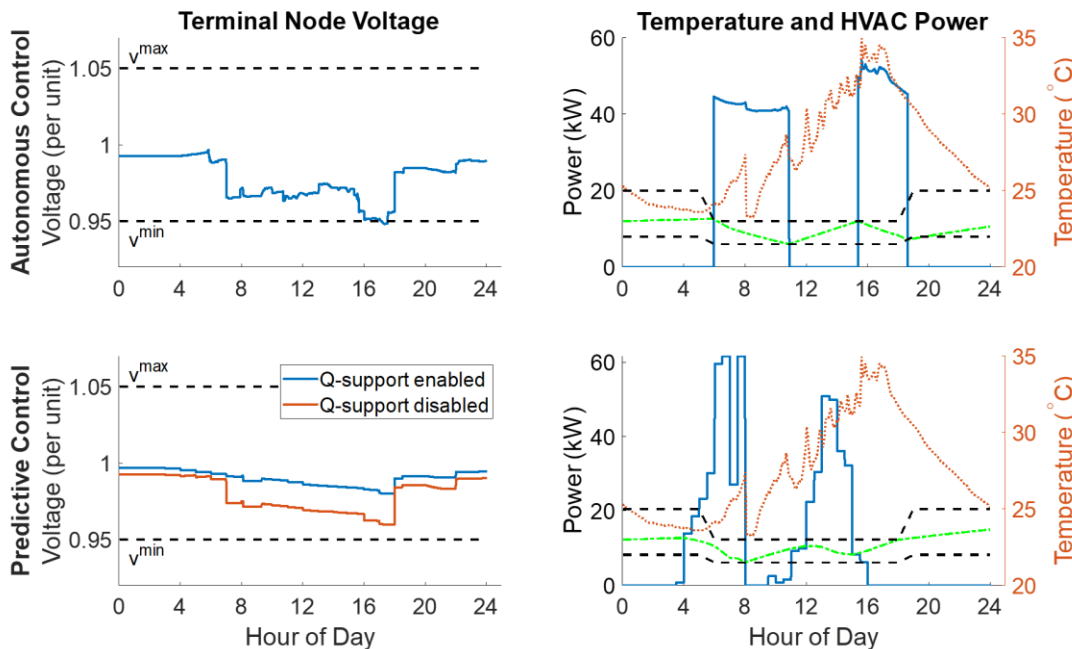


Figure 4 Simulation results – voltage and HVAC power

voltage issues before they occur, exhibiting a behavior analogous to pre-cooling a space prior to a steep increase in outdoor temperature. This smoothed voltage profile leads to increased grid stability and reliability and ensures that customers will not experience a drop in power quality during times of peak load.

When controlled by MPC, the building's peak load increases compared to the RBC; this is due to the lack of energy pricing data. Since energy is the same price at all times of day from the controller's perspective, there is no incentive to reduce peak usage (time-variable energy pricing will be introduced in future work). Additionally, the MPC controller exhibits pre-cooling behavior during the early hours of the morning, resulting in a peak of greater magnitude but shorter duration than the RBC. We also note that the MPC maintains a smoother temperature profile throughout the day thanks to its predictive ability, whereas the RBC allows the temperature to reach (and in some cases violate) the set-point before taking corrective action.

In Figure 5, the top and bottom rows show the results for RBC and MPC simulations, respectively. The three columns show battery active, battery reactive, and PV reactive power profiles for a single commercial building. (In this figure, positive values indicate power injection into the grid; negative values indicate power consumption.) Similarly to Figure 4, the predictive control plots show results for two scenarios – with and without Q-

support. Under the RBC algorithm, the battery discharges once around 4:00 pm (when the outdoor temperature and consequently building load are greatest) and charges briefly in the middle of the night. Under the MPC algorithms, however, the battery discharges and recharges throughout the day in smaller quantities; this allows the battery to provide more flexible active power support to the building while also providing reactive power support to the distribution network (when Q-support is enabled). As the figure shows, both the battery and PV inverter act as reactive sources for most of the day, injecting reactive power to the distribution network to maintain voltages as close to unity as possible.

Table 1 presents further results of this simulation study – specifically, the average thermal line losses and total energy use under each algorithm. Even without reactive power support, the centralized MPC algorithm without Q-support improves the performance of the distribution network (losses are improved) and the building (energy use is reduced) by 28.7 and 24.2 percent respectively. Once Q-support is enabled, the MPC algorithm achieves an additional 11.3 percent improvement in average thermal losses for a total of 40 percent savings over the baseline case. These results strongly demonstrate how the centralized nature of the control algorithm works to its advantage, as the controller is aware of the states of all components throughout the network and implements actions that maximize the benefit to the entire system.

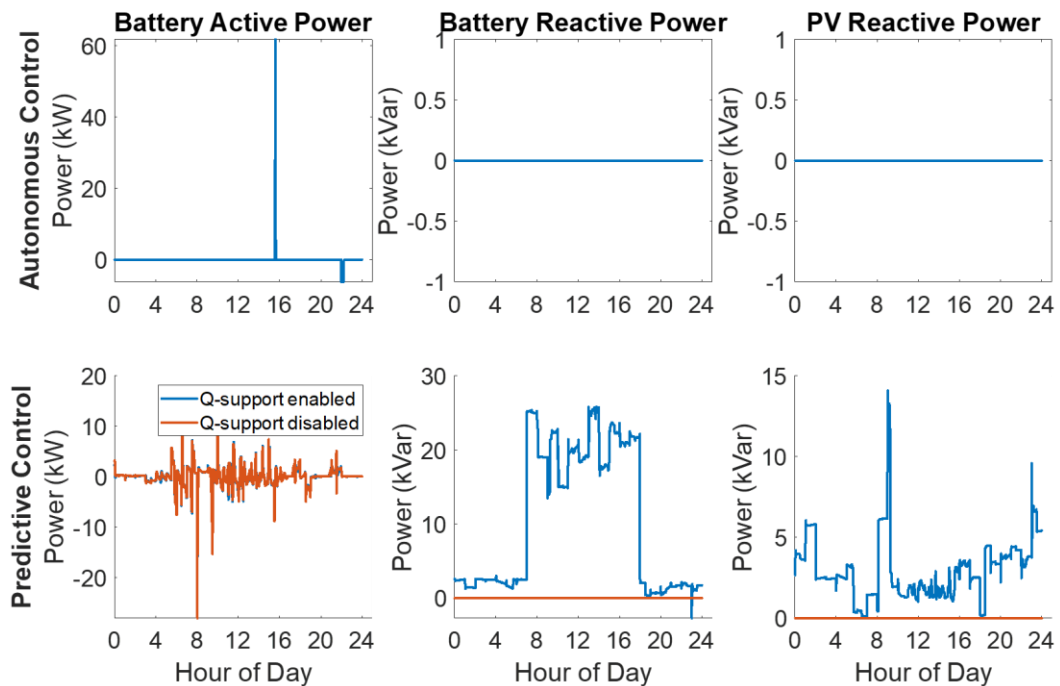


Figure 5 Simulation results – battery and PV power

Table 1 Comparison of control algorithms

ALGORITHM	LOSSES (kW)	ENERGY (kWh)
RBC	3.10	5520
MPC (Q disabled)	2.21	4184
MPC (Q enabled)	1.86	4180
Improvement	(28.7) 40.0 %	(24.2) 24.3 %

CONCLUSION

This paper presents a flexible framework for integrating buildings and distributed energy resources including PV generation devices and battery energy storage devices into the power distribution network. The framework couples the distribution network together with the building control actions and operational decisions. A centralized model predictive control algorithm is applied to the framework in order to optimally control a small network in a simulation study. The results of the study demonstrate the utility and advantage of the framework as well as the centralized controller.

This pilot study is limited in two ways. Firstly, though the developed framework is flexible enough to accommodate different types of building thermal models and differing levels of PV and battery penetration, those features were not explored in this study – each building is modeled using the same model (with different parameter values) and each building is furthermore assumed to have an associated PV device and battery. Secondly, this study does not include a sensitivity analysis of the framework and controller to different initial values and uncertainty in the disturbances (i.e., a perfect forecast is assumed). Future extensions of this work will close these two gaps, as well as expanding the size of the simulation studies to include benchmark networks and comparing the control algorithm performance to more sophisticated baseline algorithms.

Besides the two limitations already mentioned, there are two other considerations that are less pressing yet nevertheless of interest. The first is the trade-off between centralized and decentralized control. In general, centralized control results in better objective function values than decentralized control, while requiring greater computational time and resources due to the large amount of data that must be stored and manipulated. Additionally, centralized control places a higher communication burden on the entire system, as each component must send its state data to the controller at each time-step. This trade-off will be explored in a future extension of this study. The second consideration is that of implementation. Many existing buildings lack the necessary infrastructure, sensors, and equipment to implement advanced building controls such as MPC. Exploration of this challenge is currently outside the scope of this work.

ACKNOWLEDGMENT

This work was supported by the U.S. National Science Foundation under Award No. 1949372 and Award No. 1847125.

NOMENCLATURE

Model parameters

R_1, R_2, R_{win}	Building envelope thermal resistances	m^2K/W
C, C_{zone}	Building thermal conductances	W/m^2K
k_g	Discretized time-step length	s
T_{sb}	Discretization sampling time	s
$S_{bat}^{max}, S_{pv}^{max}$	(Battery, PV) inverter apparent power rating	VA
r, x	Line (resistance, reactance)	Ω
$\rho_{loss}, \rho_{\epsilon_b}$	(Distribution network, building) objective weight	–
T_p	Prediction horizon	s
T_h	Horizon receding distance	s

Model states

T_{wall}, T_{zone}	Building (wall, zone) temperature	K
SOC	Battery state of charge	–

Model variables

p_{hvac}	HVAC active power	W
p_{bat}, q_{bat}	Battery (active, reactive) power	W, Var
q_{pv}	PV reactive power	Var
α_{pv}	PV curtailment ratio	–
v	Nodal voltage	V_{pu}
P	Line active power flow	W
Q	Line reactive power flow	Var
ϵ_b	Temperature set-point violation	K

Model disturbances

T_{amb}	Ambient temperature	K
$\dot{Q}_{sol}, \dot{Q}_{int}$	(Solar, Internal) heat gains	W
p_{pv}	PV active power	W
p_{misc}, q_{misc}	Miscellaneous (active, reactive) power load	W, Var
p_{BL}, q_{BL}	Base (active, reactive) load	W, Var

Indices

k	Node index
l	Building index

REFERENCES

- ANSI. 2016. ANSI C84.1-2016 Electric Power Systems and Equipment – Voltage Ratings (60 Hz).
- Badings, Thom S., Vahab Rostampour, and Jacquelin M.A. Scherpen. 2019. “Distributed building energy storage units for frequency control service in power systems.” IFAC CSGRES. Jeju, Korea. 228–233.
- Baran, Mesut, and Felix F. Wu. 1989. “Optimal sizing of capacitors placed on a radial distribution system.” IEEE Trans. Power Delivery 4 (1): 735–743.
- Bazrafshan, Mohammadhafez, and Nikolaos Gatsis. 2018. “Comprehensive modeling of three-phase distribution systems via the bus admittance matrix.” IEEE Trans. Power Systems 33 (2): 2015–2029.
- DOE. 2011. Building Energy Data Book. Retrieved from <https://openei.org/doe-opendata/dataset/buildings-energy-data-book>.
- DOE. 2014. “Buildings-to-grid technical opportunities: Introduction and vision.” Retrieved from <https://energy.gov/eere/buildings/buildings-grid-integration>.
- DOE. 2019. EnergyPlus Essentials. Retrieved from <https://energyplus.net/documentation>.
- Farivar, Masoud, Christopher R. Clarke, Steven H. Low, and K. Mani Chandy. 2011. “Inverter VAR control for distribution systems with renewables.” Proc. IEEE SmartGridComm. Brussels, Belgium. 457–462.
- Grant, Michael, and Stephen Boyd. 2014. CVX: Matlab Software for Disciplined Convex Programming, version 2.1. Retrieved from <http://cvxr.com/cvx>.
- Gurobi Optimization, LLC. 2019. Gurobi Optimizer Reference Manual. Retrieved from <https://www.gurobi.com/documentation/9.0/refman/index.html>.
- IEEE PES Industry Technical Support Task Force. 2018. Impact of IEEE 1547 standard on smart inverter.
- Jiang, Tao, Zening Li, Xiaolong Jin, Houhe Chen, Xue Li, and Yunfei Mu. 2018. “Flexible operation of active distribution network using integrated smart buildings with heating, ventilation and air-conditioning systems.” Ap. Energy 226: 181–196.
- Kekatos, Vassilis, Gang Wang, Antonio J. Conejo, and Georgios B. Giannakis. 2015. “Stochastic reactive power management in microgrids with renewables.” IEEE Trans. Power Systems 30 (6): 3386–3395.
- Lin, Yashen, Timothy Middelkoop, and Prabir Barooah. 2012. “Identification of control-oriented thermal models of rooms in multi-room buildings.” Proc. IEEE CDC. Maui, USA. 10–13.
- Liu, Guodong, Tao Jiang, Thomas B. Ollis, Xiaohu Zhang, and Kevin Tomsovic. 2019. “Distributed energy management for community microgrids considering network operational constraints and building thermal dynamics.” Ap. Energy 239: 83–95.
- Liu, Guodong, Thomas B. Ollis, Bailu Xiao, Xiaohu Zhang, and Kevin Tomsovic. 2017. “Community microgrid scheduling considering network operational constraints and building thermal dynamics.” Energies 10 (10): 1554.
- Liu, Yang, Nanpeng Yu, Wei Wang, Xiaohong Guan, Zhanbo Xu, Bing Dong, and Ting Liu. 2018. “Coordinating the operations of smart buildings in smart grids.” Ap. Energy 228: 2510–2525.
- Mirakhorli, Amin, and Bing Dong. 2018. “Model predictive control for building loads connected with a residential distribution grid.” Ap. Energy 230: 627–642.
- Olama, Mohammed, Teja Kuruganti, James Nutaro, and Jin Dong. 2018. “Coordination and control of building HVAC systems to provide frequency regulation to the electric grid.” Energies 11 (7): 1852.
- Razmara, Meysam, Guna R. Bharati, Mahdi Shahbakhti, Sumit Paudyal, and Rush D. Robinett. 2018. “Bilevel optimization framework for smart building-to-grid systems.” IEEE Trans. Smart Grid 9 (2): 582–593.
- Smith, J. W., W. Sunderman, R. Dugan, and Brian Seal. 2011. “Smart inverter volt/var control functions for high penetration of PV on distribution systems.” Proc. IEEE/PES PSCE. Phoenix, USA. 1–6.
- Taha, Ahmad F., Nikolaos Gatsis, Bing Dong, Ankur Pipri, and Zhaoxuan Li. 2019. “Buildings-to-grid integration framework.” IEEE Trans. Smart Grid 10 (2): 1237–1249.
- Torabi, Roham, Alvaro Gomes, and F. Morgado-Dias. 2018. “The duck curve characteristic and storage requirements for greening the island of Porto Santo.” Proc. IEEE ES2DE. Funchal, Madeira. 1–7.
- Turitsyn, Konstantin, Petr Sulc, Scott Backhaus, and Michael Chertkov. 2011. “Options for control of reactive power by distributed photovoltaic generators.” Proc. IEEE 99 (6): 1063–1073.
- Wang, Gang, Vassilis Kekatos, Antonio J. Conejo, and Georgios B. Giannakis. 2016. “Ergodic energy management leveraging resource variability in distribution grids.” IEEE Trans. Power Systems 31 (6): 4765–4775.
- Wei, Tianshu, Qi Zhu, and Nanpeng Yu. 2016. “Proactive demand participation of smart buildings in smart grid.” IEEE Trans. Computers 65 (5): 1392–1405.